

Article

Effects of Temperature on Spodumene Flotation and Gas–Liquid Interface of Sodium Oleate Solutions

Ning Sun ^{1,2}, Yuhua Wang ^{1,2,*}, Ying Zhang ¹, Haoran Chu ³, Dongfang Lu ¹ and Xiayu Zheng ¹

¹ School of Minerals Processing & Bioengineering, Central South University, Changsha 410083, China; ningsun@csu.edu.cn (N.S.); 225601033@csu.edu.cn (Y.Z.); ludongfang@csu.edu.cn (D.L.); 19601229xiayu@163.com (X.Z.)

² State Key Laboratory of Mineral Processing, Beijing 102628, China

³ Zhengzhou Institute of Multipurpose Utilization of Mineral Resources, CAGS, Zhengzhou 450006, China; chuhor@mail.cgs.gov.cn

* Correspondence: wangyh@csu.edu.cn

Abstract: This study investigates the negative impact of temperature on spodumene flotation from the perspective of the gas–liquid interface of sodium oleate (NaOL) solutions. Micro-flotation tests revealed a significant decrease in the flotation recovery of spodumene when NaOL was employed as a collector, dropping from 55.3% at 305.4 K to 5.1% at 277.3 K as the temperature decreased. A strong linear correlation between the surface tension of the NaOL solution and temperature was established. As the temperature decreased, the surface tension of 6×10^{-5} mol/L NaOL increased from 37.88 mN/m at 294.9 K to 40.71 mN/m at 281.9 K, while its critical micelle concentration decreased from 9.49×10^{-4} mol/L at 305.0 K to 6.85×10^{-4} mol/L at 288.0 K. Additionally, molecular dynamics (MD) simulations indicated that a decrease in temperature resulted in an enhancement of intermolecular action forces, a more compacted interfacial structure, and weakened molecular thermal motion at the gas–liquid interface of the NaOL solution. These variations were found to be the main reason for the rise in the surface tension of the NaOL solution as the temperature decreased, which in turn lowered its efficiency, resulting in a decrease in the flotation efficiency of spodumene.



Citation: Sun, N.; Wang, Y.; Zhang, Y.; Chu, H.; Lu, D.; Zheng, X. Effects of Temperature on Spodumene Flotation and Gas–Liquid Interface of Sodium Oleate Solutions. *Minerals* **2024**, *14*, 380. <https://doi.org/10.3390/min14040380>

Academic Editor: Lev Filippov

Received: 29 February 2024

Revised: 27 March 2024

Accepted: 3 April 2024

Published: 4 April 2024



Copyright: © 2024 by the authors. Licensee MDPI, Basel, Switzerland. This article is an open access article distributed under the terms and conditions of the Creative Commons Attribution (CC BY) license (<https://creativecommons.org/licenses/by/4.0/>).

Keywords: spodumene flotation; temperature; surface tension; molecular dynamics simulation

1. Introduction

Spodumene, the main resource utilized for lithium extraction [1], is predominantly located in high-altitude regions exceeding 4000 m in China [2]. These regions are characterized by consistently low temperatures and atmospheric pressure. In industrial practice [3], it has been observed that the flotation performance of spodumene deteriorates as the temperature drops. Therefore, understanding the impact of the environmental factors in high-altitude regions, especially the temperature, on spodumene flotation is crucial for investigating new flotation collectors to efficiently exploit spodumene in these areas.

The impact of temperature on the flotation process is a critical area of research within mineral processing. Previous studies [4] have shown that fluctuations in temperature significantly alter the physicochemical properties of both mineral particles and reagents, as well as their interactions. Firstly, temperature impacts the performance of flotation reagents and their solutions [5]. Under low-temperature conditions, the solubility of collectors decreases, particularly fatty acids, resulting in their reduced activity. This leads to a decrease in their adsorption capacity on the mineral's surface. Secondly, temperature affects the viscosity and density of the flotation pulp [6]. A lower temperature increases the viscosity and density of the flotation pulp, thereby reducing pulp fluidity and affecting the dispersion of mineral particles. Thirdly, temperature influences the formation of flotation bubbles and foam stability [6,7]. As temperature drops, high-viscosity solutions reduce bubble stability. Moreover, lower temperatures lead to an increase in bubble size,

reducing the collision probability of bubbles with mineral particles. Lastly, temperature affects the kinetics of flotation [8]. A lower temperature slows the chemical reaction rates during flotation processes such as collector–mineral surface adsorption reactions, thereby extending flotation time. It should be noted that the effect of temperature on flotation has always been reciprocal rather than independent. To enhance flotation efficiency at lower temperatures, strategies typically involve augmenting the dosage of the collector or adopting high-temperature processes [9], but these cause an increase in production costs. Numerous studies have substantiated that the addition of cationic or non-ionic surfactants, such as amines [10], ether amines [11], amides [12], alkenes [13], and Gemini surfactants [14], can improve the collecting performance of anionic surfactants, and particularly fatty acids, at lower temperatures, thereby augmenting the flotation recovery of minerals. The trend of collector modification and mixed collectors signifies a crucial research focus which aims at tackling the difficulties linked to low-temperature flotation processes.

Various interface interactions during the flotation process have significant effects on flotation, while the influence of temperature on the flotation process can also be attributed to the influence of temperature on gas–liquid, solid–liquid, and solid–liquid–gas interfaces [15]. The collector not only alters the hydrophobicity of the mineral’s surface but also influences the characteristics of the flotation foam. Consequently, investigating the self-assembly process of the collector at the gas–liquid interface is integral to understanding the mineral’s flotation mechanism. The gas–liquid interface interaction during the flotation process is typically analyzed using techniques including surface tension measurements, interface structure examinations, frothiness assessments [16], and other relevant methods. Surface tension is a pivotal property of the collector solution, profoundly affecting the action at the gas–liquid interface during flotation. During the flotation process, the introduction of surfactants reduces the surface tension of the pulp solution, thereby augmenting the floatability of mineral particles. An examination of the microscopic mechanisms underlying surface tension provides insights into its nature and how temperature influences surface tension by altering intermolecular interactions.

The complexity of the gas–liquid interface arises from the intricate interplay of electrostatic, polarization, and van der Waals interactions at the molecular level [17,18]. Molecular simulation offers the advantage of dissecting individual interactions in appropriately selected systems, enabling a detailed analysis of their impact on the interface’s properties [19]. Experimentally, determining the surface composition of liquid mixtures presents challenges due to the highly disordered, non-uniform nature of the interfacial region, which is typically only a few molecular diameters thick. Nevertheless, MD simulation provides a more direct means of obtaining the distribution of molecules at the interface [20]. Further efforts are needed to establish a direct correlation between simulation results and experimental observations. Therefore, our objective was to quantitatively investigate the impact of surfactants on surface tension.

Numerous studies have been conducted on spodumene flotation, including on the characteristics of spodumene collectors [21], adsorption mechanisms [22], surface dissolution [23], isomorphous substitution, and grinding methods [24]. Nevertheless, the effect of the environmental factors in high-altitude regions on the spodumene flotation process, such as temperature and atmospheric pressure, remains largely unexplored. This study aims to integrate experimental research with computational simulations of the gas–liquid interface interactions occurring during the flotation process to elucidate the mechanisms by which temperature factors influence spodumene flotation. Our main experiments include micro-flotation tests, surface tension tests, and MD simulations.

2. Materials and Methods

2.1. Materials and Reagents

Pure spodumene samples were crushed, ground, and screened into particles of sizes ranging from 0.038 to 0.074 mm. Table 1 provides the chemical analysis results for pure spodumene samples, while Figure 1 illustrates the X-ray diffraction analysis outcomes. The Li_2O grade of the pure spodumene mineral sample is 7.90%, and its calculated purity is 98.01%. Furthermore, the XRD pattern of the spodumene samples exhibits primary peaks of spodumene and no miscellaneous peaks.

Table 1. Chemical components of spodumene samples.

Components	SiO_2	Al_2O_3	Li_2O	K_2O	Na_2O	Fe_2O_3	CaO
Mass fractions (%)	61.31	30.04	7.90	0.17	0.28	0.21	0.09

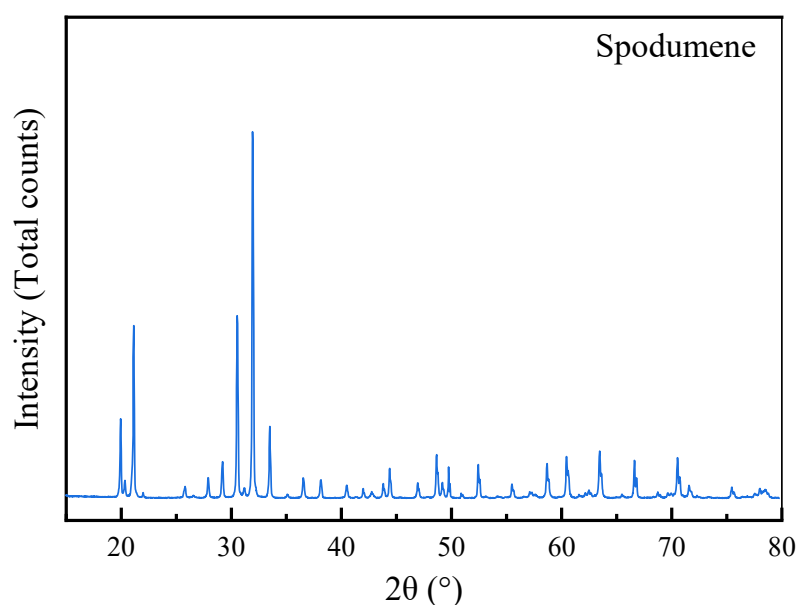


Figure 1. XRD diffraction patterns of spodumene sample.

Sodium oleate (NaOL) (AR) was used as the collector in the pure mineral flotation and surface tension tests. Sodium hydroxide (NaOH) (AR) and hydrochloric acid (HCl) (AR) were used to adjust the pH in the flotation experiments. Deionized water (DI water) with an electrical conductivity of $18.2 \text{ MΩ}\cdot\text{cm}^{-1}$ was used in both the single mineral flotation and surface tension tests.

2.2. Micro-Flotation Tests

The flotation experiments were carried out using a 40 mL self-made temperature-adjustable micro-flotation cell featuring a double-layer design. A constant-temperature water bath was deployed to regulate the temperature of the pulp within the flotation cell, thereby ensuring uniform temperature conditions throughout the flotation process. Spodumene samples weighing 3.0 g were placed in the flotation cell and subsequently filled with deionized water. After the addition of NaOL , the pulp was stirred for 4 min. HCl and NaOH were added to adjust the pH to 8.5 ± 0.5 [21]. Aired flotation was then conducted for 5 min. The foam product and tailings were filtrated, dried, and weighed individually to calculate the flotation recovery of spodumene.

2.3. Surface Tension Tests

The surface tension of the NaOL aqueous solutions was determined using the Wilhelmy Plate Method, and an automatic tension apparatus, BZY-2, with an accuracy of $\pm 0.1 \text{ mNm}^{-1}$ was used. Measurements were taken five times, and the average value was calculated. The repeatability effect was then analyzed after the test. By systematically evaluating the surface tension at different concentrations and plotting the resulting curve, the critical micelle concentration (CMC) value can be determined based on the inflection point of the curve.

2.4. Molecular Dynamics Simulations

2.4.1. Construction of Models

MD simulations were performed using Material Studio 2023 (MS). The NaOL molecular model was built using the Visualizer module. Following this, density functional theory was used to simulate the electronic structure and energetics of NaOL molecules. This allowed for the achievement of a stable chemical structure with no virtual frequency in the DMol³ module, as shown in Figure 2.

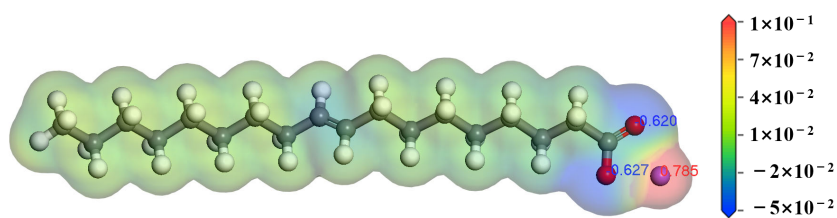


Figure 2. Charge and electrostatic potential of NaOL molecular geometric optimization model. (color codes: Red—O, Gray—C, White—H, and Modena—Na).

The Amorphous Cell module within MS was utilized to construct crystal packages for the gas phase, water phase, and NaOL monolayer, based on the density of water under different temperature conditions. Due to this vast difference in densities, the contribution of air and water vapor molecules to the system's overall density is negligible compared to that of liquid water. In simulations primarily concerned with the properties and behavior of liquid water, the effects of air and water vapor molecules in the gas phase are often considered minor compared to the interactions within the liquid phase itself. NaOL molecules possess hydrophilic groups ($-\text{COO}^-$) and hydrophobic carbon chains, leading them to preferentially aggregate at the surface of the solution. This preference results in a higher concentration of NaOL at the gas–liquid interface compared to in the liquid phase. In investigating the gas–liquid interface properties of the NaOL solution, our primary focus shifts to analyzing the concentration disparity of NaOL between the gas–liquid interface and the liquid phase. Therefore, excluding these components simplifies the system without significantly affecting the accuracy of the simulation results. At the same time, the limitations of this simulation are explained.

All the crystal packages are amalgamated into a box using the Build layer tool in the Visualizer module, thereby forming an air–surfactant–water–surfactant–air double gas–liquid interface system. It is important to note that the NaOL monolayers are aligned along the z-axis direction. The hydrophilic groups are proximal to the water layer, while the hydrophobic groups are near the gas layer, as depicted in Figure 3.

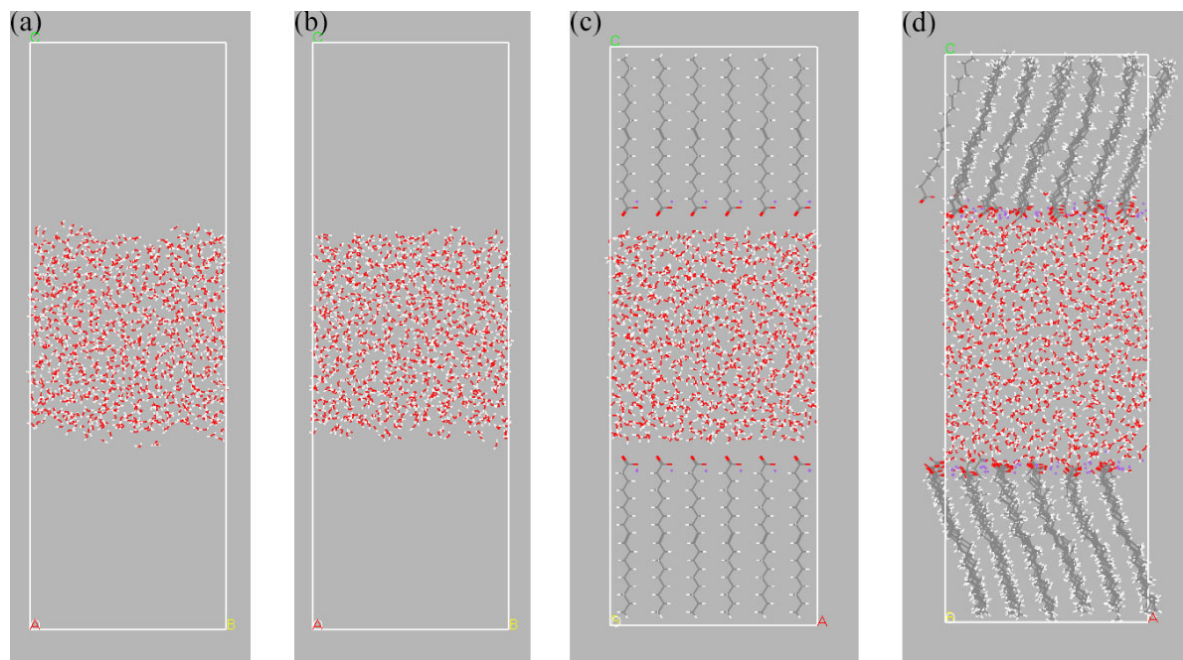


Figure 3. Simulation cells of the gas–liquid interface (color codes: Red—O, Gray—C, White—H, and Modena—Na). (a) Optimization model of the water system; (b) dynamic equilibrium of the water system; (c) optimization model of the NaOL solution system; (d) dynamic equilibrium of the NaOL solution system. White letter O: origin; Red letter A: X-axis; Yellow letter B: Y-axis; Green letter C: Z-axis.

2.4.2. Simulation Details

The geometry of the model constructed within the Forcite module was optimized utilizing the Smart algorithm. The forcefield employed for this procedure was COMPASS III. The Coulomb and Van der Waals forces were computed using the Ewald summation method, with the Cutoff distance set to 12.5 Å. The convergence tolerance energy was established at 0.0001 kcal/mol, the force at 0.005 kcal/mol/Å, and the displacement at 5×10^{-5} Å. Upon achieving convergence in both structure and energy optimization, the target systems were executed using the Dynamics tool within the Forcite module for a duration of 4 ns, with a time step of 1 fs, under the canonical ensemble. The system temperature was regulated using a Nosé–Hoover thermostat. Dynamic data from the final 1 ns were subsequently utilized for further analysis.

2.4.3. Simulation Limitations

The MD simulation is based on an ideal model (Section 2.4.1), and the accuracy and applicability of the results are limited by this model and our calculation errors. Notwithstanding these limitations, MD simulations remain a highly valuable tool for uncovering molecular-level structures and dynamic behaviors. This paper combines experimental data and theoretical simulation results to comprehensively understand the properties and behaviors of gas–liquid interfaces.

3. Results and Discussion

3.1. Effect of Temperature on Spodumene Flotation

The correlation between the NaOL dosage and flotation recovery of spodumene at 298.0 K (25.0 °C), as well as the correlation between spodumene flotation recovery and pulp temperature within a 2×10^{-4} mol/L NaOL solution, are presented in Figure 4. The flotation pulp's pH was maintained at 8.5 ± 0.5 by pH regulators.

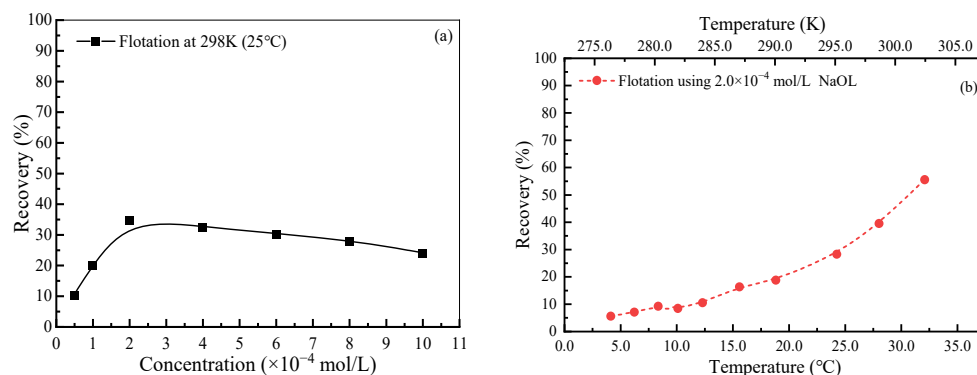


Figure 4. Flotation recovery of spodumene. (a) Black squared line: spodumene flotation at 298.0 K (25 °C), (b) red dotted line: different temperatures in 2×10^{-4} mol/L NaOL solution.

As shown in Figure 4, the flotation recovery of spodumene initially increased before decreasing with the increase in NaOL dosage, reaching its peak value of 34.5% at a concentration of 2×10^{-4} mol/L NaOL. At this optimal NaOL dosage, the flotation recovery of spodumene consistently declined from 55.3% to 5.1% as the pulp temperature decreases from 305.4 K (32.3 °C) to 277.3 K (4.2 °C).

The flotation tests demonstrated the significant impact of pulp temperature on the flotation recovery of spodumene while using NaOL as the collector. Subsequently, the influence of pulp temperature on spodumene flotation was studied based on the gas-liquid interface effect of the NaOL solution, including the surface tension and CMC of the NaOL solution.

3.2. Effect of Temperature on the Surface Tension and CMC of NaOL Solution

Figure 5 illustrates the surface tension of deionized water and NaOL solution at a concentration of 6×10^{-5} mol/L as a function of temperature. The results clearly show that the surface tension of the NaOL solution is significantly lower than that of deionized water. Additionally, the surface tension of the deionized water and 6×10^{-5} mol/L NaOL solution exhibits a strong linear relationship with temperature within the range of 308.2 K to 273.2 K. With a decreasing temperature, the surface tension of the NaOL solution increases from 37.88 mN/m at 294.9 K to 40.71 mN/m at 281.9 K.

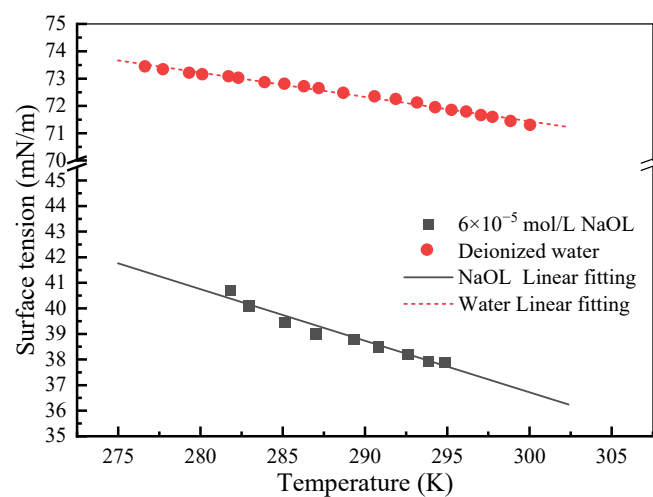


Figure 5. The surface tension of deionized water and NaOL solution with a concentration of 6×10^{-5} mol/L as a function of temperature.

Moreover, the surface tension of NaOL solution, as a function of concentration under different temperatures, is shown in Figure 6. At different temperatures, the surface tension

of the NaOL solution decreases as the NaOL concentration increases. However, the surface tension of the NaOL solution ceases to decrease at a certain concentration, whatever the temperature. At these inflection points, the surface tension of the NaOL solution is minimal, and the corresponding concentration of the NaOL solution is its CMC. Therefore, the surface tension of the NaOL solution attains its lowest value of 24.37 mN/m when the temperature is 305.0 K and the CMC of the NaOL solution is 9.49×10^{-4} mol/L. Similarly, the CMC of the NaOL solution is 7.84×10^{-4} mol/L and 6.85×10^{-4} mol/L when the temperature is 295.0 K and 288.0 K, respectively, with corresponding surface tensions of 25.13 mN/m and 25.5 mN/m observed.

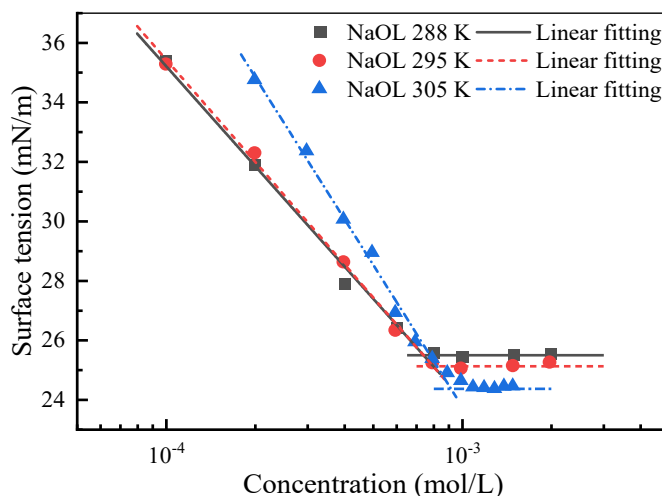


Figure 6. The relationship between the surface tension and concentration of a NaOL solution at different temperatures.

The CMC is a vital surfactant property that serves as a gauge of its surface activity. As the temperature decreases, the CMC of the NaOL solution decreases as well, leading to a reduction in the concentration needed to achieve monomolecular layer saturation adsorption and an increase in surface tension. Consequently, in the low-temperature conditions prevalent in high-altitude regions, the solution's surface tension rises while its CMC decreases, contributing significantly to the reduced flotation efficiency of spodumene. This phenomenon underscores the importance of considering temperature when optimizing flotation processes for spodumene.

Theoretically, the variations of the surface tension of the NaOL solution with temperature are the results of the interaction between NaOL molecules and water molecules at the gas–liquid interface. Therefore, further research was conducted on the molecular interaction behavior at the gas–liquid interface of the NaOL solution.

3.3. Effect of Temperature on Intermolecular Interactions

Hydrogen bonds refer to the interactions between hydrogen atoms and more electronegative atoms like oxygen, nitrogen, or fluorine. They influence the strength of the interactions at the gas–liquid interface and the arrangement of molecular structures. The higher the quantity of hydrogen bonds, the shorter the bond length, the larger the bond angle, and the stronger the intermolecular interaction becomes.

Figures 7–9 illustrate the quantity and structural characteristics of hydrogen bonds formed in water and NaOL solution systems. The characteristics of the hydrogen bonds between water molecules in water system (Figure 3b) are depicted in Figure 7. On average, each water molecule forms 3.61 hydrogen bonds, with a bond length of 1.87 Å and a bond angle of 158.50° at 298.0 K. When decreasing the temperature from 308.0 K to 278.0 K, the number of hydrogen bonds per water molecule increases from 3.578 to 3.684, the hydrogen bond length decreases from 1.873 Å to 1.853 Å, and the hydrogen bond angle increases from 158.10° to 159.43° in the water system.

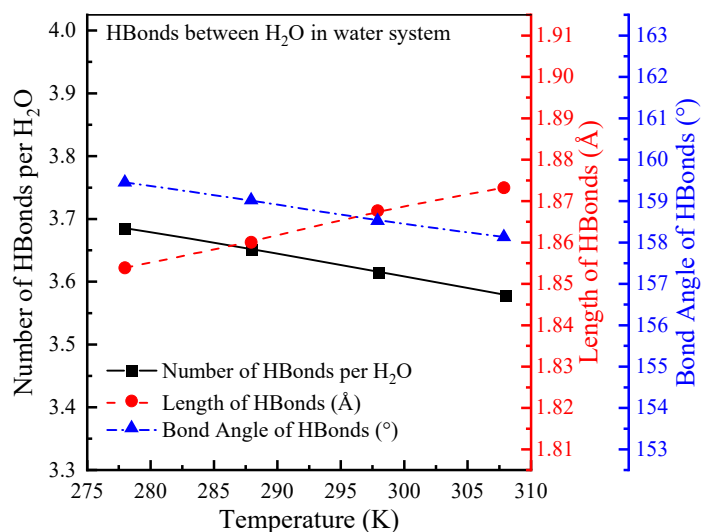


Figure 7. Properties of the hydrogen bonds between H_2O molecules in a water system, as a function of temperature.

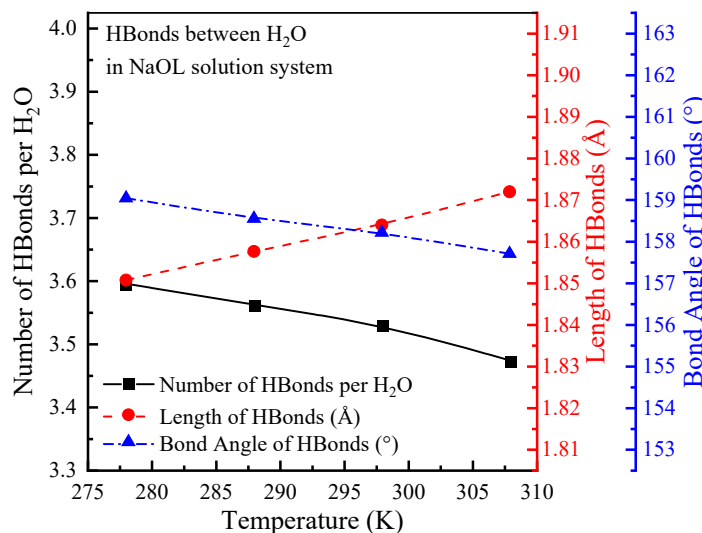


Figure 8. Properties of the hydrogen bonds between H_2O molecules in a NaOL solution system, as a function of temperature.

As shown in Figure 8, the number of hydrogen bonds between water molecules decreases by 0.09 (2.44%) in the NaOL solution system (Figure 3d), but no significant changes are observed in hydrogen bond length or angle. This indicates that part of the water molecule is squeezed out by NaOL at the gas–liquid interface, forming a hydrogen bond between NaOL and H_2O . The hydrogen bonds of $\text{H}_2\text{O}-\text{H}_2\text{O}$ and NaOL- H_2O in the NaOL solution system are shown in Figure 9. As a result, the total number of hydrogen bonds per water molecule increases by 0.1974 (5.46 %), while the bond length decreases by 0.0183 Å (0.98%) and the bond angle is reduced by 0.7417° (0.47%). The decrease in the hydrogen bond length and bond angle means that there is a stronger interaction between NaOL and water molecules than between individual water molecules. With decreasing the temperature from 308.0 K to 278.0 K, the number of all hydrogen bonds ($\text{H}_2\text{O}-\text{H}_2\text{O}$ and NaOL- H_2O) observed per water molecule increases from 3.776 to 3.880 in the NaOL solution system, the hydrogen bond length decreases from 1.856 Å to 1.838 Å, and the hydrogen bond angle increases from 157.228° to 158.475°.

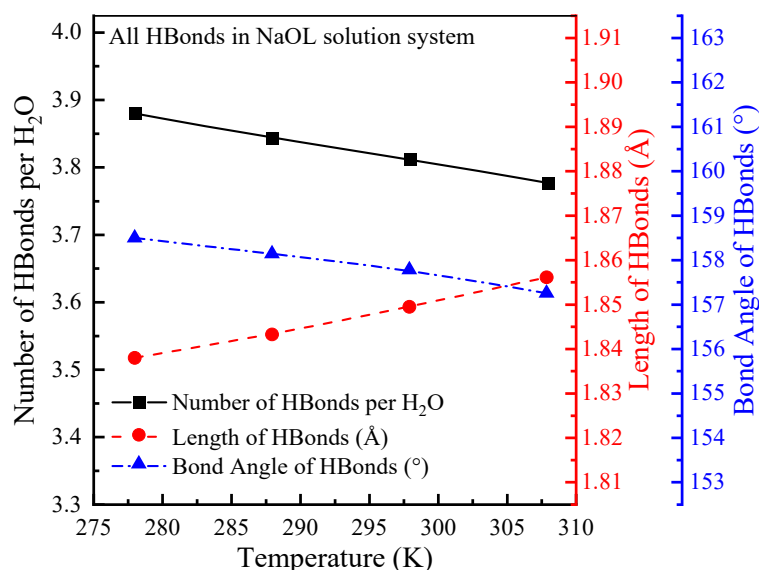


Figure 9. Properties of all hydrogen bonds of $\text{H}_2\text{O}-\text{H}_2\text{O}$ and NaOL- H_2O in a NaOL solution system, as a function of temperature.

Therefore, with the decrease in temperature, both the water system and the NaOL solution system exhibit an increase in the number of hydrogen bonds, a decrease in bond length, and an increase in bond angle. This suggests an enhancement in the strength of the hydrogen bonds, thereby increasing the surface tension at gas–liquid interfaces.

3.4. Effect of Temperature on the Gas–Liquid Interface’s Structure

Figures 10 and 11, respectively, depict the density profiles of water and NaOL molecules along the z axis of Figure 3, starting from the origin at the bottom of the cell, under varying temperature conditions in the water simulation system and NaOL simulation system.

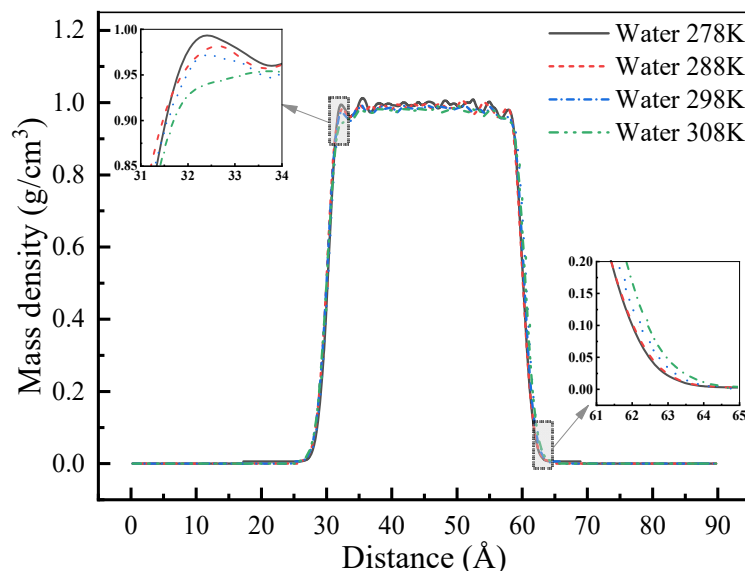


Figure 10. The density profiles of the water system along the z axis, at different temperatures.

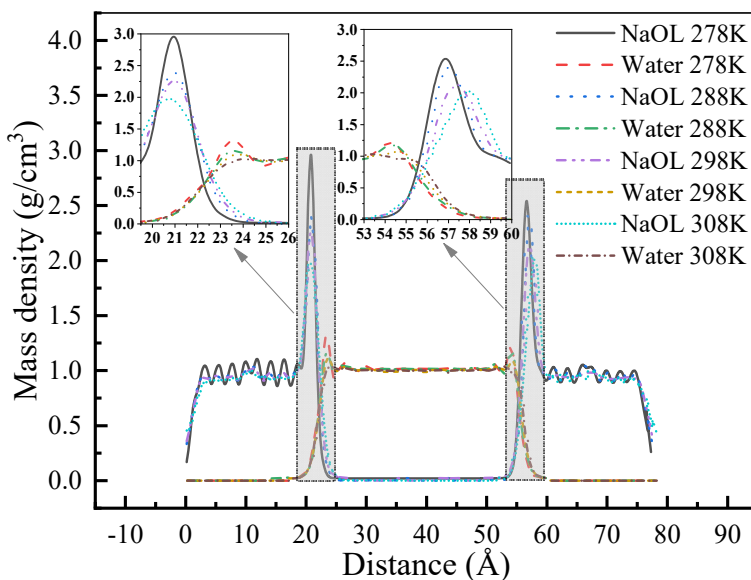


Figure 11. The density profiles of the NaOL solution system along the z axis, at different temperatures.

As shown in Figure 10, it is clear from the density profiles of the water system that two well-defined gas–liquid interfaces are established. There is a bulk liquid region of approximately 30 Å thickness between the two interfaces, and its profile is symmetric around the middle of the slab. The gas phase density is 0 g/cm³, ranging between the 0–26 Å and 64.5–90 Å intervals, while the bulk liquid phase density is about 1.0 g/cm³ in the range of 32.5–58 Å. The thickness [25] of both gas–liquid interfaces is 3 Å, respectively, spanning from 28.5 Å to 31.5 Å and from 59 Å to 62 Å. As the temperature decreases, the density profile curve of the gas–liquid interface shifts to the center, and the density profile curve of the bulk liquid phase moves upward. Consequently, the density of the bulk liquid phase decreases and the gas–liquid interface’s thickness increases, in the water system, as the temperature increases.

Figure 11 illustrates the density profiles of NaOL and H₂O at different temperatures, while the NaOL solution MD simulation system reaches equilibrium. Upon examining the density profile curve of the NaOL component at 298.0 K, within the 0–24.5 Å and 53–77.5 Å ranges, the density progressively increases, followed by a decrease, indicating that there are two NaOL monomolecular interfacial films and that their thickness is 24.5 Å. Concurrently, it is evident that the two prominent peaks in the density profiles of the NaOL solution system, observed at 21 Å and 57.5 Å, correspond to the carboxyl group (-COO⁻) in the NaOL molecules. For the density profile curve of the H₂O component at 298.0 K, an initial rise in density is noted between the 20–23 Å and 55.5–58.5 Å ranges which then reaches equilibrium. This region signifies the interface thickness of the water phase, aligning with findings in the water system. Unlike our earlier observations, the primary peaks appeared at 24 Å and 55 Å, significantly higher than the original primary peak in the water system, due to the carboxyl hydrophilicity of NaOL, which caused the aggregation of water molecules. Additionally, two mixed regions exist where both water and NaOL molecules combine, in the 20–24.5 Å and 54–58.5 Å ranges. Within these regions, these segments of NaOL molecules interact with water molecules, reflecting that their hydrophilic polar group is being combined with water molecules. With a decrease in temperature, the main peak of the density profile curve increases in height, decreases in width, and shifts to the center. This suggests that the arrangement of molecules on the surface becomes more compact and that the thickness of the interface between the water and NaOL constituents becomes narrower.

These aforementioned experiments indicate that, in both single water and NaOL systems, a decrease in temperature results in an increased formation of hydrogen bonds characterized by shorter bond lengths and larger bond angles. This enhanced intermolecu-

lar interaction leads to an increase in solution density and a decrease in interface thickness and intermolecular spacing, consequently increasing the surface tension of the solutions under low-temperature conditions.

Contrastingly, the arrangement of the surfactants and water molecules was investigated through the analysis of the radial distribution function (RDF) of the H_2O and $-\text{COO}^-$ constituents in the NaOL solution system, which is illustrated in Figure 12. The RDF of water exhibits two peaks at radii of 1.05 Å and 1.69 Å, which represent the first and second dense water molecular layers encircling a fixed water molecule. The RDF of the $-\text{COO}^-$ constituent displays two significant peaks at radii of 1.23 Å and 2.23 Å. These peaks represent the first and second dense carboxyl layers surrounding a fixed carboxyl. Significantly, both the RDF curves of the H_2O and $-\text{COO}^-$ constituents exhibit a consistent pattern such that as the temperature decreases, the value of the main peak increases and its width diminishes, indicating strengthened molecular interactions, thereby elevating the surface tension of the NaOL solution.

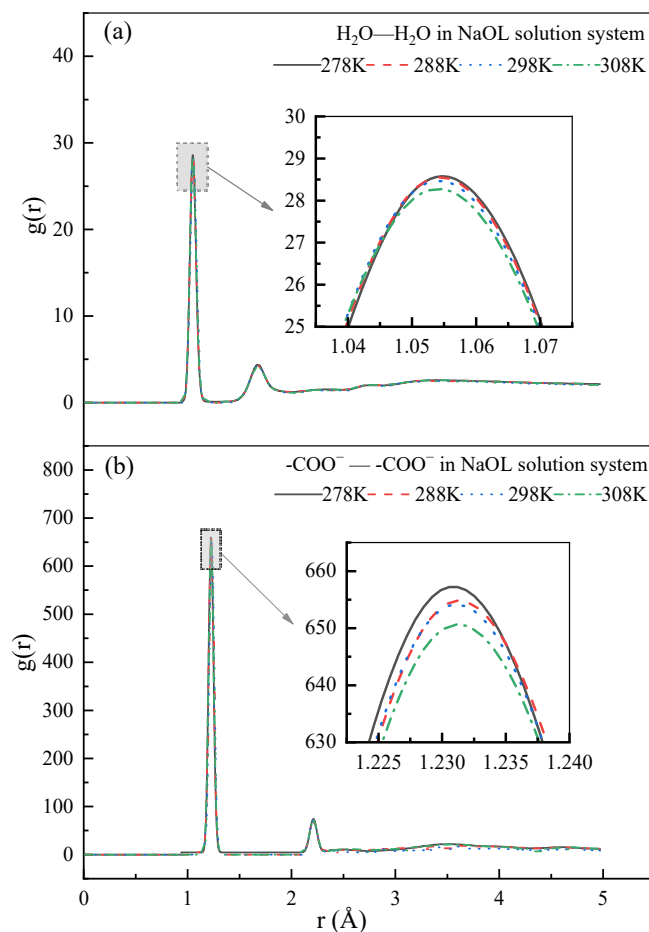


Figure 12. The RDFs of intermolecular H_2O and $-\text{COO}^-$ in the NaOL solution system at different temperatures: (a) H_2O — H_2O ; (b) $-\text{COO}^-$ — $-\text{COO}^-$.

3.5. Effect of Temperature on Molecular Thermal Motion

Based on the mean square displacement analysis of the H_2O and NaOL molecules in the water and NaOL solution systems, the relationship between the diffusion coefficient of these molecules (H_2O and NaOL molecules) and temperature is presented in Figure 13. At each temperature, the diffusion coefficient of the water molecules in the NaOL system is approximately 30% lower than that in the water system. The amphiphilic structure of NaOL promotes its aggregation at the interface, leading to the interaction between its head group and water molecules at the interface, forming hydrogen bonds. Consequently, the water molecules at the interface transition from "free water" to "bound water". The

diffusion coefficient of water molecules in the water solution system exhibits a gradual decrease from $0.25755 \text{ \AA}^2/\text{ps}$ at 308.0 K to $0.16387 \text{ \AA}^2/\text{ps}$ at 278.0 K . As the temperature drops from 308.0 K to 278.0 K , the diffusion coefficient of the water molecules decreases from $0.1943 \text{ \AA}^2/\text{ps}$ to $0.10422 \text{ \AA}^2/\text{ps}$ and the diffusion coefficient of the NaOL molecules shows a reduction from $0.00561 \text{ \AA}^2/\text{ps}$ to $0.00199 \text{ \AA}^2/\text{ps}$, in the NaOL solution system.

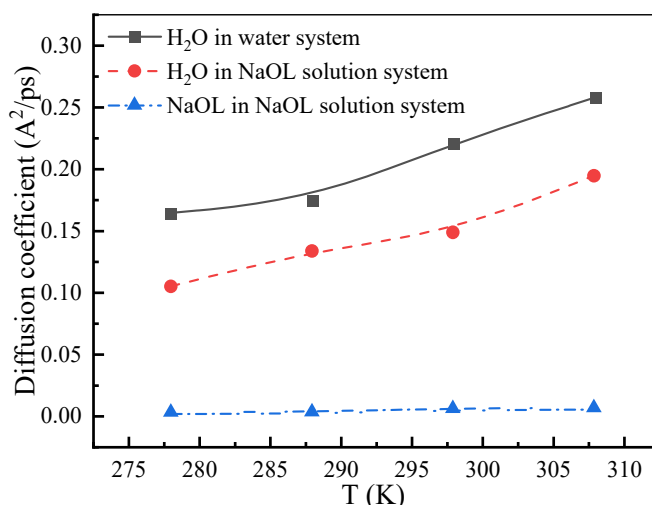


Figure 13. Diffusion coefficient of NaOL and water molecules as a function of temperature in different solution systems.

Consequently, the decrease in the molecular thermal motion in the NaOL solution system as the temperature decreases reduces the probability of intermolecular hydrogen bond rupture. This stability enhances intermolecular interactions, thereby elevating the surface tension of the NaOL solution.

4. Conclusions

This research investigated the effect of temperature on spodumene flotation in NaOL systems by employing both experimental studies and MD simulations. Micro-flotation tests revealed that a decrease in temperature from 305.4 K to 277.3 K resulted in a significant decrease, from 55.3% to 5.1%, in the floatation recovery of spodumene.

The decrease in temperature from 294.9 K to 281.9 K resulted in an increase in the surface tension of the NaOL solution, from 37.88 to 40.71 mN/m . Simultaneously, its CMC decreased from $9.49 \times 10^{-4} \text{ mol/L}$ at 305.0 K to $6.85 \times 10^{-4} \text{ mol/L}$ at 288.0 K . The rise in the surface tension of the NaOL solution with decreasing temperature, reflecting a decline in the collecting efficiency of NaOL, emerges as the primary factor contributing to the reduced flotation recovery of spodumene at lower temperatures.

The study of the intermolecular interaction forces reveals that a decrease in temperature leads to an increase in the number of hydrogen bonds, a decrease in the length of the hydrogen bonds, and an increase in the angle of the hydrogen bonds in the NaOL solution. The results concerning the interfacial structure of the solution demonstrate that lowering the temperature leads to decreased intermolecular spacing, increased density, and reduced interface thickness. The results of molecular thermal motion indicated that decreasing the temperature caused a reduction in the diffusion coefficient of molecules within the NaOL solution. These changes strengthen the intermolecular interactions at the interface, ultimately increasing the surface tension and consequently diminishing the collecting performance of the NaOL solution. Despite the limitations of the ideal model, MD simulation studies have convincingly shown that low temperatures impact the gas–liquid interface’s molecular interactions, structure, and molecular thermal motion. This is one of the mechanisms contributing to the challenges in collector performance, and spodumene flotation specifically, in high-altitude and cold regions.

5. Future Works

In high-altitude regions, the environmental factors that have negative effects on spodumene flotation are not only temperature but also atmospheric pressure, air humidity, oxygen content, and so on. Exploring the impacts of these factors is a novel and promising research avenue for future studies. While this paper primarily addresses the influence of temperature on spodumene flotation, with a focus on the gas–liquid interface, future research will expand on this to include the solid–liquid interface and the gas–liquid–solid three-phase interface. This will encompass aspects such as reagent and mineral adsorption, as well as the processes of the collision, adsorption, and desorption of bubbles from particles. These foundational studies aim to develop reagents and process services suitable for flotation recovery in cold high-altitude regions, with the ultimate goal of efficiently exploiting the resources in these areas.

Author Contributions: Conceptualization, N.S. and Y.W.; methodology, N.S.; formal analysis, N.S.; investigation, N.S. and Y.Z.; resources, Y.W.; data curation, N.S.; writing—original draft preparation, N.S.; writing—review and editing, Y.W., H.C. and N.S.; supervision, Y.W., D.L. and X.Z.; project administration, Y.W.; funding acquisition, Y.W. All authors have read and agreed to the published version of the manuscript.

Funding: This research was funded by the National Natural Science Foundations of China, grant number 52174267, and the Open Foundation of State Key Laboratory of Mineral Processing, grant number BGRIMM-KJSKL-2023-18.

Data Availability Statement: The data are contained within the article.

Acknowledgments: This work was supported, in part, by the High Performance Computing Center of Central South University.

Conflicts of Interest: The authors declare no conflicts of interest.

References

1. Salakjani, N.K.; Singh, P.; Nikoloski, A.N. Production of lithium—A literature review. Part 2. Extraction from spodumene. *Min. Proc. Ext. Met. Rev.* **2021**, *42*, 268–283. [[CrossRef](#)]
2. Zhang, B.; Qi, F.Y.; Gao, X.Z.; Li, X.L.; Shang, Y.T.; Kong, Z.Y.; Jia, L.Q.; Meng, J.; Guo, H.; Fang, F.K.; et al. Geological characteristics, metallogenetic regularity, and research progress of lithium deposits in China. *China Geol.* **2022**, *4*, 734–767. [[CrossRef](#)]
3. Li, S.; Lu, D.; Chen, X.; Zheng, X.; Li, X.; Chu, H.; Wang, Y. Industrial application of a modified pilot-scale jameson cell for the flotation of spodumene ore in high altitude area. *Powder Technol.* **2017**, *320*, 358–361. [[CrossRef](#)]
4. Wang, C.; Man, X.; Ou, L. Molecular dynamics study of the effect of temperature on the flotation behavior of sodium oleate on the surface of diaspore. *Miner. Eng.* **2023**, *192*, 108004. [[CrossRef](#)]
5. An, D.; Zhang, J. A study of temperature effect on the xanthate’s performance during chalcopyrite flotation. *Minerals* **2020**, *10*, 426. [[CrossRef](#)]
6. Zhang, W.; Nesson, J.E.; Finch, J.A. Bubble size as a function of some situational variables in mechanical flotation machines. *J. Cent. South Univ.* **2014**, *21*, 720–727. [[CrossRef](#)]
7. Zhang, Y.; Sam, A.; Finch, J.A. Temperature effect on single bubble velocity profile in water and surfactant solution. *Colloids Surf. A Physicochem. Eng. Asp.* **2003**, *223*, 45–54. [[CrossRef](#)]
8. Feng, D.; Aldrich, C. Influence of operating parameters on the flotation of apatite. *Miner. Eng.* **2004**, *17*, 453–455. [[CrossRef](#)]
9. Kang, J.; Liu, Y.; Khoso, S.A.; Hu, Y.; Sun, W.; Liu, R. Significant improvement in the scheelite heating flotation with sodium sulfide. *Minerals* **2018**, *8*, 587. [[CrossRef](#)]
10. Luo, B.; Zhu, Y.; Sun, C.; Li, Y.; Han, Y. The flotation behavior and adsorption mechanisms of 2-((2-(decyloxy)ethyl)amino)lauric acid on quartz surface. *Miner. Eng.* **2018**, *117*, 121–126. [[CrossRef](#)]
11. Liu, X.; Xie, J.; Huang, G.; Li, C. Low-temperature performance of cationic collector undecyl propyl ether amine for ilmenite flotation. *Miner. Eng.* **2017**, *114*, 50–56. [[CrossRef](#)]
12. Guo, W.; Han, Y.; Zhu, Y.; Li, Y.; Tang, Z. Effect of amide group on the flotation performance of lauric acid. *Appl. Surf. Sci.* **2020**, *505*, 144627. [[CrossRef](#)]
13. Chen, C.; Zhu, H.; Sun, W.; Hu, Y.; Qin, W.; Liu, R. Synergetic effect of the mixed anionic/non-ionic collectors in low temperature flotation of scheelite. *Minerals* **2017**, *7*, 87. [[CrossRef](#)]
14. Ni, C.; Xie, Y.; Liu, C.; Han, Z.; Shen, H.; Ran, W.; Xie, W.; Liang, Y. Exploring the separation mechanism of gemini surfactant in scheelite froth flotation at low temperatures: Surface characterization, DFT calculations and kinetic simulations. *Sep. Purif. Technol.* **2023**, *305*, 122358. [[CrossRef](#)]

15. Cao, S.; Yin, W.; Yang, B.; Zhu, Z.; Sun, H.; Sheng, Q.; Chen, K. Insights into the influence of temperature on the adsorption behavior of sodium oleate and its response to flotation of quartz. *Int. J. Min. Sci. Technol.* **2022**, *32*, 399–409. [[CrossRef](#)]
16. Luo, X.; Qi, L.; Wen, S.; Wang, Y.; Lai, H.; Lin, Q.; Zhou, Y.; Wu, X.; Song, Z. Adsorption configuration of dodecylamine at gas–liquid interface and its relationship with foam stability: Md simulation and tof-sims investigation. *Miner. Eng.* **2021**, *164*, 106830. [[CrossRef](#)]
17. Van der Waals, J.D. The thermodynamik theory of capillarity under the hypothesis of a continuous variation of density. *J. Stat. Phys.* **1979**, *20*, 197–200. [[CrossRef](#)]
18. Everett, D.H. (Ed.) *What Is the Role of Surface Chemistry? Surface Tension and Adsorption*; The Royal Society of Chemistry: London, UK, 1988. [[CrossRef](#)]
19. Joslin, C.G.; Gray, C.G.; Chapman, W.G.; Gubbins, K.E. Theory and simulation of associating liquid mixtures. *Fluid Mol. Phys.* **1987**, *62*, 843–860. [[CrossRef](#)]
20. Zhu, G.; Liu, R.; Wang, X.; Miller, J.D.; Cao, Y. Molecular characteristics of the mixed cationic/anionic collector interface probed by sum-frequency vibrational spectroscopy and molecular dynamics simulations. *J. Mol. Liq.* **2023**, *385*, 122408. [[CrossRef](#)]
21. Cook, B.K.; Gibson, C.E. A review of fatty acid collectors: Implications for spodumene flotation. *Minerals* **2023**, *13*, 212. [[CrossRef](#)]
22. Filippov, L.; Farrokhpay, S.; Lyo, L.; Filippova, I. Spodumene flotation mechanism. *Minerals* **2019**, *9*, 372. [[CrossRef](#)]
23. Wang, Y.; Sun, N.; Chu, H.; Zheng, X.; Lu, D.; Zheng, H. Surface dissolution behavior and its influences on the flotation separation of spodumene from silicates. *Sep. Sci. Technol.* **2021**, *56*, 1407–1417. [[CrossRef](#)]
24. Zhu, G.; Wang, Y.; Wang, X.; Miller, J.D.; Lu, D.; Zheng, X.; Zhao, Y.; Zheng, H. Effects of grinding environment and lattice impurities on spodumene flotation. *T. Nonferr. Metal. Soc.* **2019**, *29*, 1527–1537. [[CrossRef](#)]
25. Taylor, R.S.; Dang, L.X.; Garrett, B.C. Molecular dynamics simulations of the liquid/vapor interface of spc/e water. *J. Phys. Chem.* **1996**, *100*, 11720–11725. [[CrossRef](#)]

Disclaimer/Publisher's Note: The statements, opinions and data contained in all publications are solely those of the individual author(s) and contributor(s) and not of MDPI and/or the editor(s). MDPI and/or the editor(s) disclaim responsibility for any injury to people or property resulting from any ideas, methods, instructions or products referred to in the content.